

LETTER TO THE EDITOR

# Can we trace very cold dust from its emission alone ? \*

L. Pagani<sup>1,2</sup>, C. Lefèvre<sup>1,2</sup>, M. Juvela<sup>3</sup>, V.-M. Pelkonen<sup>3,4</sup>, and F. Schuller<sup>5</sup>

<sup>1</sup> LERMA, Observatoire de Paris, PSL Research University, CNRS, UMR 8112, F-75014 Paris, France  
e-mail: laurent.pagani@obspm.fr

<sup>2</sup> Sorbonne Universités, UPMC Univ. Paris 6, UMR 8112, LERMA, F-75005, Paris, France

<sup>3</sup> Department of Physics, P.O.Box 64, FI-00014, University of Helsinki, Finland, mika.juvela@helsinki.fi

<sup>4</sup> Finnish Centre for Astronomy with ESO (FINCA), University of Turku, Väisäläntie 20, FI-21500 Piikkiö, Finland

<sup>5</sup> European Southern Observatory, Alonso de Córdova 3107, Vitacura, Casilla 19001, Santiago de Chile, Chile

Received 02/10/2014; accepted 23/12/2014

## ABSTRACT

**Context.** Dust is a good tracer of cold dark clouds but its column density is difficult to quantify.

**Aims.** We want to check whether the far-infrared and submillimeter high-resolution data from *Herschel* SPIRE and PACS cameras combined with ground-based telescope bolometers allow us to retrieve the whole dust content of cold dark clouds.

**Methods.** We compare far-infrared and submillimeter emission across L183 to the 8  $\mu\text{m}$  absorption map from Spitzer data and fit modified blackbody functions towards three different positions.

**Results.** We find that none of the *Herschel* SPIRE channels follow the cold dust profile seen in absorption. Even the ground-based submillimeter telescope observations, although more closely following the absorption profile, cannot help to characterize the cold dust without external information such as the dust column density itself. The difference in dust opacity can reach up to a factor of 3 in prestellar cores of high extinction.

**Conclusions.** In dark clouds, the amount of very cold dust cannot be measured from its emission alone. In particular, studies of dark clouds based only on *Herschel* data can miss a large fraction of the dust content. This has an impact on core and filament density profiles, masse and stability estimates.

**Key words.** ISM: clouds – Infrared: ISM – Submillimeter: ISM – dust, extinction – ISM: individual objects : L183, L134N, L1689B

## 1. Introduction

Dark clouds are the places where stars form. We try to follow the different steps that lead from a low-density cloud to main-sequence star. Some steps have been clearly identified like the Class 0 to Class III protostar evolution (Lada 1987; Andre et al. 1993) but, the early phases, such as the (formation of a prestellar core (PSC), the collapse of this core, are still not well understood. Studies of clouds and of PSCs first attempt to determine their mass. This is not a simple task. The first difficulty is to know the distance of the object, and the second is to trace the column density of the material itself. The main components,  $\text{H}_2$  and He are not directly visible, with the exception of a little  $\text{H}_2$  seen in absorption in the UV at the cloud edges, and surrogate tracers are needed. Molecules are not good tracers in general because CO, which is the standard tracer, is depleted in the PSCs (Lemme et al. 1995; Willacy et al. 1998; Tafalla et al. 2002; Pagani et al. 2005; Brady Ford & Shirley 2011). Tracers of the PSCs like  $\text{NH}_3$  or  $\text{N}_2\text{H}^+$  do not extend beyond the PSCs themselves, and contrary to CO, their peak abundance is variable. Detailed radiative transfer models are therefore needed to retrieve the  $\text{H}_2$  + He densities via the modelling of their collisions with the tracers (followed by integration along the line of sight to obtain the total column density). On the other hand, dust is traceable from the edge of the clouds to the centre. Its relative abundance to  $\text{H}_2$  is not accurately known but is thought to be in the range  $\sim 1/130$ – $1/100$  in the Milky Way (Flower et al. 2005;

Compiègne et al. 2011). It can be traced either by its extinction of background stars (Wolf 1923; Bok 1956; Bok & Cordwell 1973) with a higher efficiency in the near-infrared (NIR, Lada et al. 1994; Lombardi & Alves 2001; Lombardi 2009) or of background diffuse light in the mid-infrared (MIR, Bacmann et al. 2000), by its scattering of the interstellar radiation field (ISRF) in the NIR and MIR (Lehtinen & Mattila 1996; Juvela et al. 2006; Lefèvre et al. 2014), or by its emission in the far-infrared (FIR) (Ward-Thompson et al. 1994). However, all these methods have difficulties. The use of background stars do not allow to reach a high spatial resolution outside the galactic plane and become absent typically when  $A_V \geq 40$  mag. Scattering is a promising but difficult method, highly dependent on the type of grains (size distribution, extinction, albedo, phase function), on the background intensity, and on the ISRF anisotropy and strength (see Lefèvre et al. 2014 for an exhaustive study). Emission depends on the knowledge of the grain properties, spectral index and temperature (e.g. Juvela & Ysard 2012 for a discussion of the degeneracy of the problem). The advantage of dust emission measurements in the FIR and submillimetre domains is that it remains optically thin up to  $N(\text{H}_2) \sim 2 \times 10^{24} \text{ cm}^{-2}$  at 300  $\mu\text{m}$  and even higher at longer wavelengths. Dust observed in emission is therefore able to trace the whole cloud content from the edge to the centre. However, it remains difficult to convert this emission into the actual column density of dust.

Before the launch of *Herschel* (Pilbratt et al. 2010), FIR measurements of dust emission in the range 200–500  $\mu\text{m}$  were scarce (e.g. Stepnik et al. 2003) and many studies limited themselves to fit the dust in emission by building single spectral energy dis-

Send offprint requests to: L. Pagani

\* see Appendix B for institutional acknowledgements

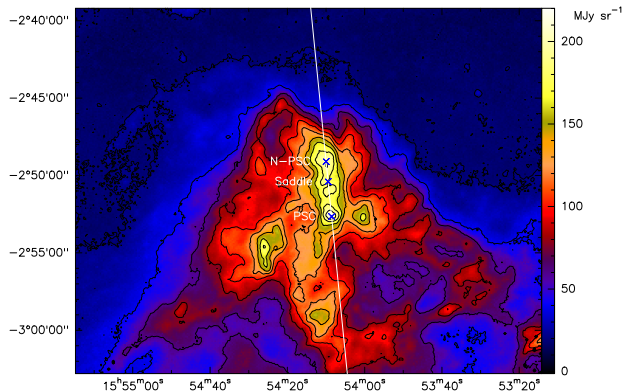


**Fig. 1.** L183 *Herschel*/SPIRE map at 250  $\mu\text{m}$ . Contour levels every 20  $\text{MJy sr}^{-1}$ . The cut through the region is traced as a  $\sim 6^\circ$  tilted line with respect to the vertical (equatorial North) direction.

tribution (SED) fits based on a mix of measurements shorter than 200  $\mu\text{m}$  and longer than 850  $\mu\text{m}$ . However, Pagani et al. (2004) showed that in a dark cloud without embedded sources, the 200  $\mu\text{m}$  emission traces only the envelope of the cloud ( $A_V \leq 7.5$  mag from the surface) and totally misses the bulk of the dust too cold to emit significantly at that wavelength. Hence, it could be deduced from that result that single SED fits were not realistic because short wavelengths are mostly tracing emission from the envelope and long wavelengths emission from the core. There was no connection between the two sides of the (modified) blackbody curve and therefore no physical meaning to that fit. The question arises again today now that all wavelengths between 100 and 1200  $\mu\text{m}$  have been sampled in a number of clouds with several telescopes, including Spitzer (Werner et al. 2004), AKARI (Murakami et al. 2007), ground-based bolometers, and above all, *Herschel* (Pilbratt et al. 2010) and *Planck* (Tauber et al. 2010), to find out if we can accurately retrieve the dust content from fitting SEDs alone. Indeed, dust at 10 K is brightest at 300  $\mu\text{m}$ , while dust as cold as 6 K is brightest at 500  $\mu\text{m}$ . Both wavelengths are inside the range observed by SPIRE, the FIR camera of *Herschel* (Griffin et al. 2010) and not far from the two highest frequency channels of *Planck*/HFI (Lamarre et al. 2010). Using *Herschel* data, Nielbock et al. (2012) achieved a successful temperature analysis of B68 but they combined data from NIR to submm. Roy et al. (2014) attempted to fit two cores (B68 and L1689B) using *Herschel* data alone. They both find temperatures lower than provided by single blackbody fittings of the SEDs. Some aspects of dust emission fitting of mock clouds have also been numerically explored by Malinen et al. (2011).

## 2. Observations

This work is based on maps of L183 taken at 8, 100, 160, 250, 350, 500, 870, and 1200  $\mu\text{m}$ . The 8  $\mu\text{m}$  data were taken with Spitzer/IRAC, Fazio et al. 2004, published in Steinacker et al. 2010). *Herschel*/PACS took the 100 and 160  $\mu\text{m}$  maps, and *Herschel*/SPIRE the 250, 350, and 500  $\mu\text{m}$  maps (Pilbratt et al. 2010; Poglitsch et al. 2010; Griffin et al. 2010). These maps are partly published in Juvela et al. (2012, for the 250  $\mu\text{m}$  data) and will be published in Montillaud et al. (2014); Juvela et al. (2014), and Lefèvre et al. (in prep.). Lefèvre et al. will also publish two new APEX/LABOCA and IRAM-30m/MAMBO maps at 870 and 1200  $\mu\text{m}$ , respectively. In this Letter, we only present a cut inclined eastward by  $\sim 6^\circ$  with respect to the vertical (Fig. 1). It

is adjusted to go through the main prestellar core (PSC) and the northern prestellar core (N-PSC, Figs. 1&2). The minimum in extinction between the two cores is named the saddle. Details about data reduction will be exposed in Lefèvre et al. (in prep.). Shortly, *Herschel* data acquired as part of the *Galactic cold cores* key project (Juvela et al. 2010) were re-reduced with the *Herschel* interactive processing environment (HIPE) v.12.1, using the official pipeline (Ott 2010), including Scanamorphos v.23 for PACS data (Roussel 2013). They were subsequently colour-corrected, zeroed, and rescaled using IRIS (Miville-Deschênes & Lagache 2005) and *Planck* data (Juvela-subm). The calibration error is a small fraction of the background subtraction uncertainty which we estimate at 10% for SPIRE and 15% for PACS. We reduced LABOCA data using BoA<sup>1</sup>, and MAMBO data using MOPSIC<sup>2</sup>. Both LABOCA and MAMBO data lack the large scale, low surface brightness part of the cloud because of the observing method of MAMBO (in-source OFF subtraction) and the data reduction method for LABOCA, which requires strong filtering to remove sky fluctuations. To recover most of the lost signal, we combined these data with *Planck* data that are colour-corrected and interpolated to match the LABOCA and MAMBO filter band-passes. For MAMBO, the correction is no more than 10%, while for LABOCA the correction amounts to 30 %. The final uncertainty is estimated to be  $\sim 20\%$  for both.

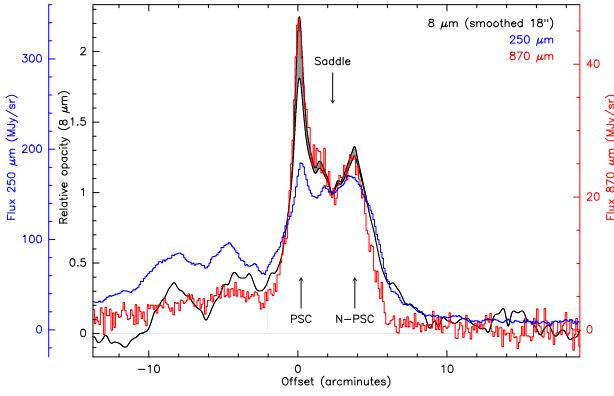
## 3. Analysis

Figure 2 shows the extinction profile along the cut (as defined in Fig. 1), derived from the 8  $\mu\text{m}$  data degraded to the resolution of, and compared with, the 250  $\mu\text{m}$  and the 870  $\mu\text{m}$  cuts. The 8  $\mu\text{m}$  opacity values are only a qualitative representation of the expected extinction. It is based on a previous estimate by Pagani et al. (2004), on the necessity to reach zero extinction at the edges of the cloud, and on the estimated ratio in column density between the PSC and the N-PSC, which is 1.5–2 at the MAMBO 12'' resolution (after smoothing to 18'', the ratio is in the range 1.4–1.7). The extinction is represented as a range between these two ratio values. These values are only indicative since the 8  $\mu\text{m}$  absorption map is in fact strongly contaminated by scattered light and cannot be safely converted to an opacity map without a 3D model taking the scattering due to micron-sized grains into account (Steinacker et al. 2010; Pagani et al. 2010; Lefèvre et al. 2014). A better estimate of the extinction based on NIR and MIR absorption and scattering, including the 8  $\mu\text{m}$  map, will be presented in Lefèvre et al. (in prep.).

While the strong features from the 8  $\mu\text{m}$  data and the 870  $\mu\text{m}$  data are clearly correlated, the weak peaks southward (negative offsets in Fig. 2) seen at 8  $\mu\text{m}$  are missing at 870  $\mu\text{m}$ . This is due to the loss of extended features with LABOCA. These features are too small to be resolved by *Planck* and are detected only as a smooth increase in emission in this *Planck*+LABOCA combined data cut. The 250  $\mu\text{m}$  emission detects the two southern peaks (with a small shift for the most opaque one, most probably due to an anisotropic heating). However, it does not correctly trace the main PSC since the main peak and the northern peak have almost the same intensity instead of the ratio 1.4–1.7 we expect from submm observations. Both peaks are also too weak compared to the saddle intensity. This is reminiscent of the similar result reported by Pagani et al. (2004) in which they showed that the ISOPHOT 200  $\mu\text{m}$  map does not follow the dust column density in the inner part of the cloud. The low resolution

<sup>1</sup> <http://www.eso.org/sci/activities/apexsv/labocasv.html>

<sup>2</sup> <http://www.iram.es/IRAMES/mainWiki/CookbookMopsic>



**Fig. 2.** L183 cut. The 8  $\mu\text{m}$  data have been smoothed to 18'' resolution to match both the *Herschel*/SPIRE 250  $\mu\text{m}$  and APEX/LABOCA 870  $\mu\text{m}$  common resolution. The 8  $\mu\text{m}$  absorption cut is converted to relative extinction (see text). The grey filling represents the possible range of 8  $\mu\text{m}$  ratio between main and northern peaks. All curves are aligned at the saddle point (at +2'33'' offset).

(90'') of the ISOPHOT map could have been a partial explanation, but it can now be seen that resolution is not an issue and the dust is simply too cold to contribute significantly to the 250  $\mu\text{m}$  emission in the central parts of the cloud. Indeed, the peak intensity ratio between the southern peak at offset -4'40'' and the two main peaks is about 2 at 250  $\mu\text{m}$ , while it is larger than 3 for the northern peak and in the range 4–5 for the main PSC in terms of relative opacity at 8  $\mu\text{m}$ . Figure 3 shows the dust emission along the cut at wavelengths from 100 to 1200  $\mu\text{m}$ . The resolution of all the data has been aligned on that of the SPIRE 500  $\mu\text{m}$  channel (37''). The longer the wavelength, the better the tracing of the two dust peaks. Figure 4 displays the SEDs for the three points of interest along the cut: the main PSC, the saddle, and the northern PSC. For all three positions, we tried to fit the SED with either two or three modified blackbodies, one at 17 K, one at  $\sim 10$  K, and an optional one at 6 K,

$$I_\nu = \sum_{i=1}^n B_\nu(T_{d,i}) \tau_{\nu_0} \left(\frac{\nu}{\nu_0}\right)^{\beta_i} = \sum_{i=1}^n B_\nu(T_{d,i}) \kappa_{\nu_0} \mu m_H N(\text{H}_2) \left(\frac{\nu}{\nu_0}\right)^{\beta_i}, \quad (1)$$

with  $n = 2$  or  $3$ . The parameter  $B_\nu$  is the Planck function at dust temperature  $T_d$ ,  $\nu_0 = 1$  THz ( $\lambda = 300$   $\mu\text{m}$ ),  $\mu = 2.33$  the mean molecular weight,  $m_H = 1.67 \times 10^{-24}$  g the proton weight,  $N(\text{H}_2)$  the gas column density, and  $\kappa_{\nu_0}$  the dust opacity at 300  $\mu\text{m}$ . The dust opacity  $\kappa_{\nu_0} = 0.111$   $\text{cm}^2 \text{g}^{-1}$  corresponds to the thin ice case at density  $1 \times 10^6 \text{cm}^{-3}$  from Ossenkopf & Henning (1994) for a gas-to-dust ratio of 133 (Compiègne et al. 2011), which is compatible with Ysard et al. (2013). The spectral index  $\beta$  describes the modification of the dust opacity  $\kappa_\nu$  with frequency. The main blackbody is optimized for all three parameters,  $T_d$ ,  $\beta$ ,  $N(\text{H}_2)$ . The cold blackbody, if included, is set at 6 K, and  $\beta$  and  $N(\text{H}_2)$  can be adjusted. The third blackbody at 17 K, with  $\beta = 1.8$ , is set to fit the grains on the cloud surface, which contribute at 100  $\mu\text{m}$ . Their only free parameter is  $N(\text{H}_2)$ . Their temperature and spectral index are typical of diffuse and cloud surface dust temperatures (Zucconi et al. 2001; Planck Collaboration 2011). Their contribution is always less than 0.3% of the total mass and is not discussed any further. We independently adjust  $\beta$  values in the range 1.5–4 with the constraint that  $\beta_{T_d} \leq \beta_{6\text{K}}$ . The fits are optimized so that  $\chi^2 \leq 0.5$  in all cases (all parameter values are in Fig. 4). The striking result is that the fit is just as good with  $n = 2$  (blackbodies at  $\sim 10$  and 17 K) or  $n = 3$  (6,  $\sim 10$ , and 17 K). The  $\chi^2$  values remain basically identical. Towards the main PSC, the

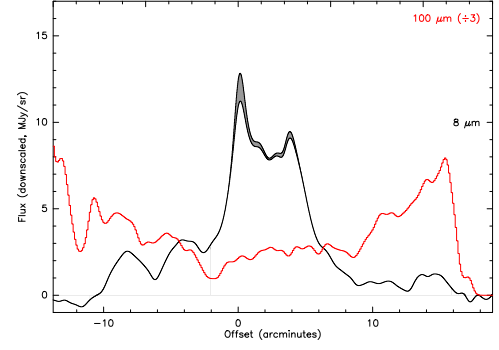


**Fig. 3.** L183 cut for dust emission. This cut includes data from *Herschel* PACS and SPIRE, APEX/LABOCA, and IRAM-30m/MAMBO data, all convolved to 37'' resolution, shown one by one. The fluxes are scaled down by the amount indicated to the right of the wavelengths to align all the fluxes on the saddle point (except at 100  $\mu\text{m}$ ). The 8  $\mu\text{m}$  opacity range is displayed (black lines filled in grey), the 250  $\mu\text{m}$  is traced in blue for easier comparison with Fig. 2. [CLICK HERE TO CHANGE WAVELENGTH](#). The FIR wavelengths (except the 100  $\mu\text{m}$  one) are shown together in the Appendix (Fig. A.1)

opacity at 300  $\mu\text{m}$  varies from  $0.02 \pm 0.07$  ( $n = 2$ ) to  $0.058$  ( $n = 3$ ), almost a factor of three, in the case presented in Fig. 4, and could go up to 0.1 (a factor of five higher) in the extreme case where  $\beta_{6\text{K}} \approx 3.9$ . As expected the difference is less for the saddle and the northern PSC but the increase in opacity can still be  $\geq 50\%$ . There is no way to discriminate between the fits simply based on these data. Of course, three blackbody fitting instead of two is still far from the real case (a continuous variation of temperature from  $\sim 17$  K at the surface of the clouds to  $\sim 6$  K in the densest cores, Zucconi et al. 2001; Evans et al. 2001) but comes much closer to it already.

The fits we find with an imposed 6 K blackbody are not unique. Since a solution can be found without a 6 K component, the opacity of this component can be varied from 0 up to 0.1 depending on the other parameters,  $T_{\text{dust}}$  and  $\beta$  in particular, with similar  $\chi^2$  values. Constraints must come from other observations, which we discuss now.

For the main PSC,  $N(\text{H}_2)$  is in the range  $4.5 \pm 1.7 \times 10^{22} \text{cm}^{-2}$  for  $n = 2$  to  $1.3^{+1.0}_{-0.8} \times 10^{23} \text{cm}^{-2}$  for  $n = 3$ . The second result encompasses the column density determined via gas modelling. Pagani et al. (2007) indicate  $N(\text{H}_2) \sim 1.0 \times 10^{23} \text{cm}^{-2}$  from  $\text{N}_2\text{H}^+$  data when averaged in a 37'' beam (after correcting for the new  $\text{N}_2\text{H}^+ - \text{H}_2$  collisional coefficients, Lique et al. 2015). However  $\text{N}_2\text{H}^+$  only traces the dense region and not the envelope of the cloud. From  $\text{C}^{18}\text{O}$  measurements (Pagani et al. 2005), we infer a cloud envelope column density of  $\sim 2 \times 10^{22} \text{cm}^{-2}$ . The total is  $\sim 1.2 \times 10^{23} \text{cm}^{-2}$ . The difference with the  $n = 2$  fit (ratio of 2.5) is larger than the different uncertainties involved here. With the new  $\text{N}_2\text{H}^+ - \text{H}_2$  collisional coefficients, we also found that the gas temperature in the core is 6 K (7 K in Pagani et al. 2007) where the density is  $\geq 5 \times 10^5 \text{cm}^{-3}$ , which is a density high enough to efficiently thermalise gas and dust ( $n > 1 \times 10^5 \text{cm}^{-3}$  is required, Goldsmith 2001). Therefore, dust and gas temperatures and column densities can be made consistent only if we introduce a 6 K dust component in the fit. Based only on *Herschel* data, Roy et al. (2014) also find a temperature lower than that given by a single SED fit (9.8 K instead of 11.6 K in the case of L1689B at its centre), and their fit is more realistic than the one we present here by using a continuously varying temperature with radius. However,

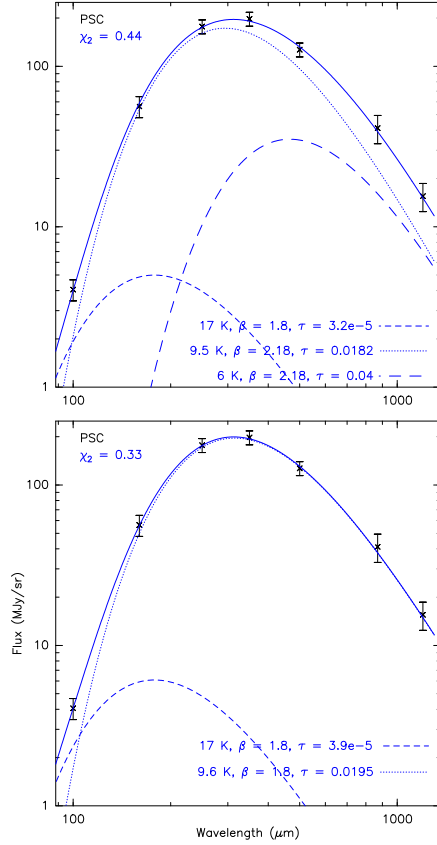


**Fig. 4.** SEDs of the three points of interest defined in Fig. 2 along the cut (in apparition order, the main PSC, the saddle and the northern PSC). Top row, the SEDs are fitted with three modified blackbodies, bottom row, with two modified blackbodies. Opacity is given at  $300 \mu\text{m}$ . [CLICK TO DISPLAY THE THREE CASES IN TURN](#). The three plots are shown separately in the Appendix (Fig. A.2).

despite this more sophisticated analysis, Roy et al.'s method fails to reveal the very cold dust (6–8 K) in the heart of L1689B that we have identified from  $\text{N}_2\text{H}^+$  measurements (Bacmann et al., in prep). These measurements indicate a  $37''$  beam-averaged column density of  $7\text{--}11 \times 10^{22} \text{ cm}^{-2}$ , again a factor 2 to 3 times higher than Roy et al.'s  $3.5 \times 10^{22} \text{ cm}^{-2}$ , which does not even take the contribution from the envelope devoid of  $\text{N}_2\text{H}^+$  emission into account. Another attempt by Marsh et al. (2014) gives better results. They trace cold dust down to 6 K but they use a priori density and temperature profiles and therefore their results somewhat depend on their input parameters in contrast with Roy et al. approach.

It is clear from these two cases that very cold dust exists and is not identified as such solely by its emission. This is because of the well-known fact that warmer dust (even as low as 10 K) outshines the very cold dust because of the non-linearity of the blackbody function (at 6 K, the Rayleigh-Jeans approximation is not valid above 100 GHz). This is clearly visible in Fig. 4 where the 6 K blackbody contribution is smaller than the  $\sim 10$  K contribution, even at  $\lambda = 1.2 \text{ mm}$  and even when it represents 70% of the total mass (45% of the signal in that case). Though L183 and L1689B could be thought of as peculiar cases, we believe they are only clear illustrations of a general problem, since dust below 9 K is predicted to occur for radial extinctions as low as  $A_V = 10 \text{ mag}$  (Zucconi et al. 2001), in standard ISRF conditions (no local heating source). It is clear that studies of filaments, and

cold dark clouds in general, based solely on dust emission (and worse, single component SED fits), even including *Herschel* or *Planck* data, should meet the degeneracy problem we expose here and will miss a large fraction of the mass in these objects. Even more sophisticated modelling, as presented by Roy et al. (2014), misses a large fraction of the mass. In the present two cases, L183 and L1689B, 30 to 70% of the total mass is lacking. The dust column density must be retrieved by other means (dust in extinction, molecular emission). Therefore, critical and threshold masses, core and filament stabilities, and density profiles in studies limited to dust emission should be considered with caution.

**Acknowledgements.** CL acknowledges financial support by the DIM ACAV and Région Île de France. MJ and V-MP acknowledge the support of Academy of Finland grant 250741. We thank the referee for her/his remarks which helped to clarify this Letter.

## References

- Andre, P., Ward-Thompson, D., & Barsony, M. 1993, *ApJ*, 406, 122  
 Bacmann, A., André, P., Puget, J.-L., et al. 2000, *A&A*, 361, 555  
 Bok, B. J. 1956, *AJ*, 61, 309  
 Bok, B. J. & Cordwell, C. S. 1973, in *Molecules in the Galactic Environment*, ed. M. A. Gordon & L. E. Snyder, 54–+  
 Brady Ford, A. & Shirley, Y. L. 2011, *ApJ*, 728, 144  
 Compiègne, M., Flagey, N., Verstraete, L., et al. 2011, *A&A*, 525, A103  
 Evans, II, N. J., Rawlings, J. M. C., Shirley, Y. L., & Mundy, L. G. 2001, *ApJ*, 557, 193  
 Fazio, G. G., Hora, J. L., Allen, L. E., et al. 2004, *ApJS*, 154, 10  
 Flower, D. R., Pineau Des Forêts, G., & Walmsley, C. M. 2005, *A&A*, 436, 933  
 Goldsmith, P. F. 2001, *ApJ*, 557, 736  
 Griffin, M. J., Abergel, A., Abreu, A., et al. 2010, *A&A*, 518, L3+  
 Juvela, M., Pelkonen, V.-M., Padoan, P., & Mattila, K. 2006, *A&A*, 457, 877  
 Juvela, M., Ristorcelli, I., Montier, L. A., et al. 2010, *A&A*, 518, L93+  
 Juvela, M., Ristorcelli, I., Pagani, L., et al. 2012, *A&A*, 541, 12  
 Juvela, M. & Ysard, N. 2012, *A&A*, 541, A33  
 Juvela, M., Demyk, K., Doy, Y., et al. 2014, *A&A*, *subm.*  
 Lada, C. J. 1987, in *IAU Symposium*, Vol. 115, *Star Forming Regions*, ed. M. Peimbert & J. Jugaku, 1–17  
 Lada, C. J., Lada, E. A., Clemens, D. P., & Bally, J. 1994, *ApJ*, 429, 694  
 Lamarre, J.-M., Puget, J.-L., Ade, P. A. R., et al. 2010, *A&A*, 520, A9  
 Lefèvre, C., Pagani, L., Juvela, M., et al. 2014, *ArXiv e-prints*  
 Lehtinen, K. & Mattila, K. 1996, *A&A*, 309, 570  
 Lemme, C., Walmsley, C. M., Wilson, T. L., & Muders, D. 1995, *A&A*, 302, 509  
 Lique, F., Daniel, F., Pagani, L., & Feautrier, N. 2015, *MNRAS*, 446, 1245  
 Lombardi, M. 2009, *A&A*, 493, 735  
 Lombardi, M. & Alves, J. 2001, *A&A*, 377, 1023  
 Malinen, J., Juvela, M., Collins, D. C., Lunttila, T., & Padoan, P. 2011, *A&A*, 1  
 Marsh, K. A., Griffin, M. J., Palmeirim, P., et al. 2014, *MNRAS*, 439, 3683  
 Miville-Deschênes, M.-A. & Lagache, G. 2005, *ApJS*, 157, 302  
 Montillaud, J., Juvela, M., Rivera-Ingraham, A., et al. 2014, *A&A*, *subm.*  
 Murakami, H., Baba, H., Barthel, P., et al. 2007, *PASJ*, 59, 369  
 Nielbock, M., Launhardt, R., Steinacker, J., et al. 2012, *A&A*, 547, A11  
 Ossenkopf, V. & Henning, T. 1994, *A&A*, 291, 943  
 Ott, S. 2010, in *Astronomical Society of the Pacific Conference Series*, Vol. 434, *Astronomical Data Analysis Software and Systems XIX*, ed. Y. Mizumoto, K.-I. Morita, & M. Ohishi, 139  
 Pagani, L., Bacmann, A., Cabrit, S., & Vastel, C. 2007, *A&A*, 467, 179  
 Pagani, L., Bacmann, A., Motte, F., et al. 2004, *A&A*, 417, 605  
 Pagani, L., Pardo, J.-R., Apponi, A. J., Bacmann, A., & Cabrit, S. 2005, *A&A*, 429, 181  
 Pagani, L., Steinacker, J., Bacmann, A., Stutz, A., & Henning, T. 2010, *Science*, 329, 1622  
 Pilbratt, G. L., Riedinger, J. R., Passvogel, T., et al. 2010, *A&A*, 518, L1+  
 Planck Collaboration. 2011, *A&A*, 536, A24  
 Poglitsch, A., Waelkens, C., Geis, N., et al. 2010, *A&A*, 518, L2+  
 Roussel, H. 2013, *PASP*, 125, 1126  
 Roy, A., André, P., Palmeirim, P., et al. 2014, *A&A*, 562, A138  
 Steinacker, J., Pagani, L., Bacmann, A., & Guieu, S. 2010, *A&A*, 511, A9+  
 Stepnik, B., Abergel, A., Bernard, J.-P., et al. 2003, *A&A*, 398, 551  
 Tafalla, M., Myers, P. C., Caselli, P., Walmsley, C. M., & Comito, C. 2002, *ApJ*, 569, 815  
 Tauber, J. A., Mandolesi, N., Puget, J.-L., et al. 2010, *A&A*, 520, A1+

- Ward-Thompson, D., Scott, P. F., Hills, R. E., & André, P. 1994, MNRAS, 268, 276
- Werner, M. W., Roellig, T. L., Low, F. J., et al. 2004, ApJS, 154, 1
- Willacy, K., Langer, W. D., & Velusamy, T. 1998, ApJ, 507, L171
- Wolf, M. 1923, Astronomische Nachrichten, 219, 109
- Ysard, N., Abergel, A., Ristorcelli, I., et al. 2013, A&A, 559, A133
- Zucconi, A., Walmsley, C. M., & Galli, D. 2001, A&A, 376, 650



## Appendix A: Multi-layered picture

Figure A.1 shows the layers of Fig. 3 assembled together for direct comparison, for pdf viewers not understanding Javascript, and for printers. Similarly, Fig. A.2 shows the layers of Fig. 4 (the three positions tested with two or three blackbody components) side by side.

## Appendix B: Institutional acknowledgements

This work is based on observations carried out with the IRAM 30m Telescope. IRAM is supported by INSU/CNRS (France), MPG (Germany), and IGN (Spain) and on data acquired with the Atacama Pathfinder Experiment (APEX). APEX is a collaboration between the Max-Planck-Institut für Radioastronomie, the European Southern Observatory, and the Onsala Space Observatory. *Planck* (<http://www.esa.int/Planck>) is a project of the European Space Agency – ESA – with instruments provided by two scientific consortia funded by ESA member states (in particular the lead countries: France and Italy) with contributions from NASA (USA), and telescope reflectors provided in a collaboration between ESA and a scientific Consortium led and funded by Denmark. *Herschel* is an ESA space observatory with science instruments provided by European-led Principal Investigator consortia and with important participation from NASA.

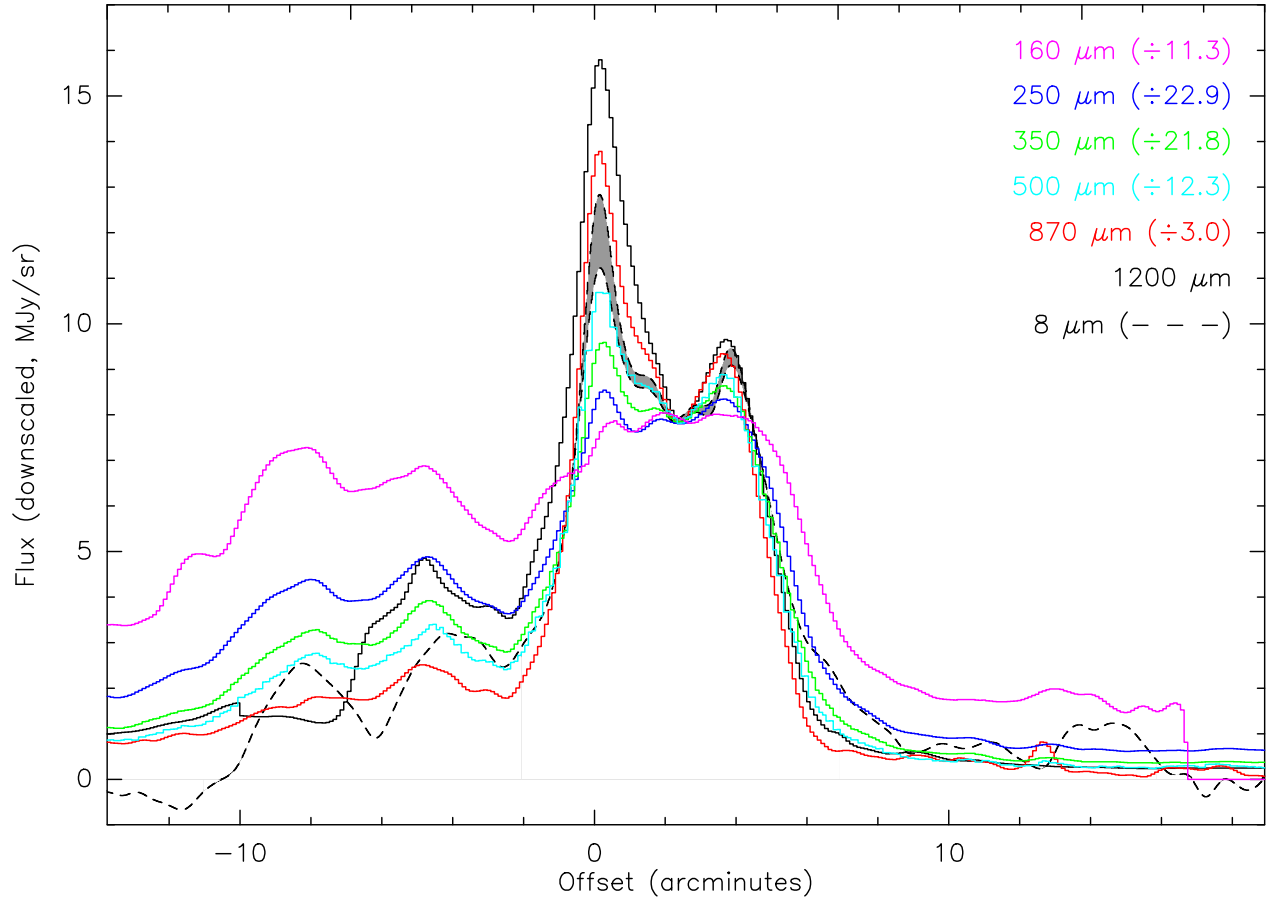


**Fig. A.1.** L183 cut for dust emission. It includes data from *Herschel* PACS and SPIRE, APEX/LABOCA, and IRAM-30m/MAMBO data, all convolved to  $37''$  resolution. The fluxes are scaled down by the amount indicated to the right of the wavelengths to align all the fluxes on the saddle point. The  $8\,\mu\text{m}$  opacity range is displayed (dashed lines filled in grey), the  $100\,\mu\text{m}$  cut is omitted since it only traces the cloud content at its surface. This is the developed version of Fig. 3. The colour is changed for each wavelength to help separate them.

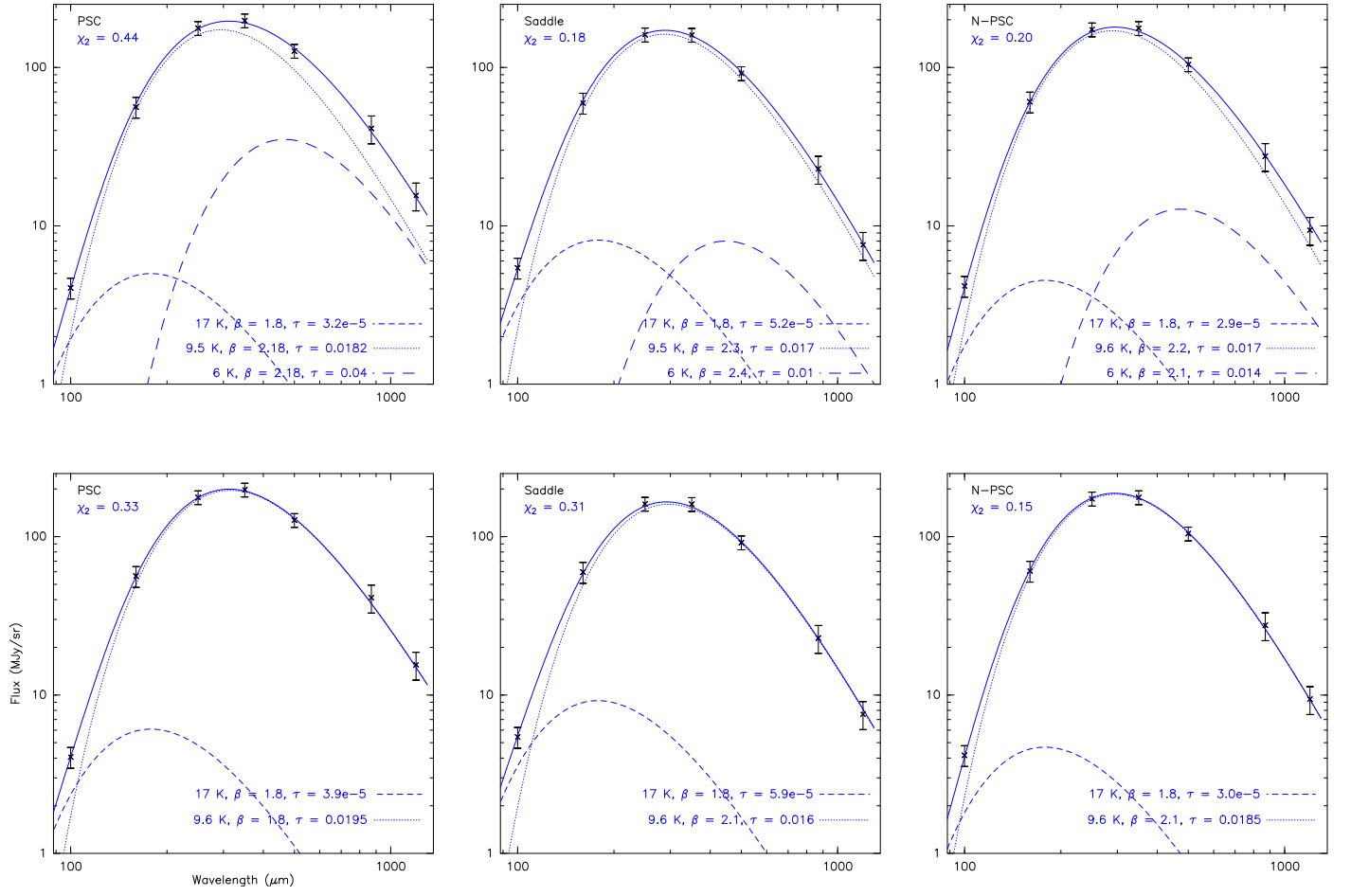


**Fig. A.2.** SEDs of the three points of interest defined in Fig. 2 along the cut (from left to right, the main PSC, the saddle and the northern PSC). Top row, the SEDs are fitted with three modified blackbodies, bottom row, they are fitted with two modified blackbodies. Opacity is given at  $300\text{ }\mu\text{m}$ . This is the developed version of Fig. 4.